Real-time Implementation and Evaluation of Magnetometerless Tracking System for Human and Humanoid Posture Control Benchmarking based on Inertial Sensors

Vittorio Lippi[a], Kai Günter Brands[b] and Thomas Seel
Technical University Berlin, Control Systems, Berlin, Germany

Keywords: Tracking System, Magnetometerless, Humanoid Posture Control, Benchmarking.

Abstract: This work describes a tracking system designed for humanoid robots, exoskeletons and humans oriented to posture control and balance experiments. The system aims to provide a tool that allows for repeatability of balance experiments across different robotics platforms and control algorithms with the ultimate aim of providing a standardized framework for performance benchmarking. To make the system suitable for different geometries and materials, it relies just on inertial sensors. The system is evaluated with a marker-based optical tracking, performing a trial of a typical posture control and balance experiment. In particular the frequency response function of the body segments respect to the support surface tilt is evaluated.

1 INTRODUCTION

Posture control and balance are fundamental components of humanoid robot control, considering the inherently unstable nature of humanoid body. COMTEST is a sub-project of the EU project EUROBENCH that aims to the development of a standardized testbed for balance performance (Lippi et al., 2019b; Lippi et al., 2019a). In this framework, the trajectory of body segments should be measured in a repeatable way with different robots. In this work, we evaluate a tracking system designed to be suitable for humans, robots, and exoskeletons regardless of materials and geometry. The target of the proposed solution are researchers and companies in the field of humanoids and wearable robots. The tracking solution can be used at the EUROBENCH facility or replicated in laboratories exploiting off-shelf tracking hardware. Posture control experiments have been performed with optical tracking e.g. (Mergner et al., 2009; Hettich et al., 2013; Hettich et al., 2015) or exploiting the same internal sensors used for the control e.g. (Lippi, 2018; Ott et al., 2016; Hauser et al., 2011) or a mixture of the two solutions e.g. (Zebenay et al., 2015). Optical tracking is considered the golden standard for body tracking (Teufl et al., 2019b) and often the chosen solution for gait and posture analysis

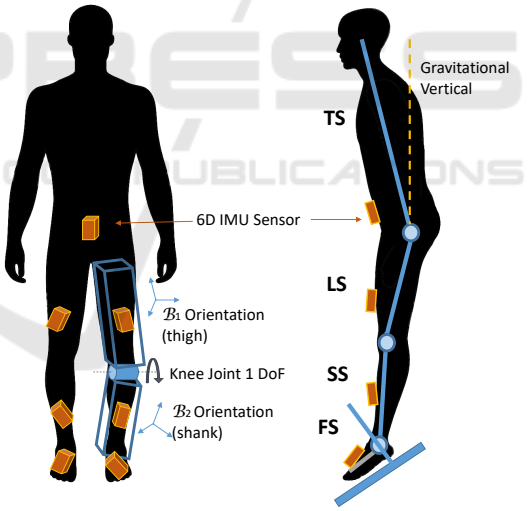

Figure 1: Placement of IMU sensors on Human/Humanoid body and body segments kinematics. On the left: the position of the 7 sensors on the body. Each sensor is fixed to a body segment that is considered rigid. The joints between segments are assumed to be 1 DoF hinge joints. The orientation of each sensor respect to the tracked body segment is not known *a priori*. On the right: the variables considered for the analysis of posture control. The sway of body segments is expressed respect to the gravitational vertical (TS = Trunk in space, LS= leg in space, SS = shank in space, FS = foot in space). FS is expressed as the orientation of the normal to the support surface, i.e. FS=0 means that the surface is horizontal.

[a] https://orcid.org/0000-0001-5520-8974
[b] https://orcid.org/0000-0003-0290-3257

Lippi, V., Brands, K. and Seel, T.
Real-time Implementation and Evaluation of Magnetometerless Tracking System for Human and Humanoid Posture Control Benchmarking based on Inertial Sensors.
DOI: 10.5220/0009869106750680
In *Proceedings of the 17th International Conference on Informatics in Control, Automation and Robotics (ICINCO 2020)*, pages 675-680
ISBN: 978-989-758-442-8

(Leardini et al., 2005). Optical tracking systems have the drawback of being expensive and limited by line-of-sight restrictions. In recent years there has been growing interest in developing cheaper body tracking systems based on inertial measurements units, IMUs (Miller et al., 2004; Fong and Chan, 2010; Buke et al., 2015; Wong et al., 2015; Salehi. and Stricker., 2020). IMUs typically require extensive calibration protocols as well as a homogeneous magnetic field (De Vries et al., 2009). The proposed tracking system will use recently developed sensor fusion methods (Laidig et al., 2017b; Seel and Ruppin, 2017) to achieve accurate real-time motion tracking in a plug-and-play manner (Laidig et al., 2017a; Müller et al., 2016; Seel et al., 2014) without relying on a homogeneous magnetic field. This tracking system is meant to be a reference that can be used also to evaluate the internal sensor fusion of the tested robot. The system specifications are designed to allow both the acquisition of the data for offline analysis and also real time operations and control, such as body-sway-referenced support surface tilt (Mergner and Lippi, 2018) and provide position feedback to human subjects. In contrast to existing solutions, the magnetometer-free tracking system is both real-time-capable and achieves automatic sensor-to-segment calibration. In this work, the system is evaluated using a marker-based optical tracking system as reference, as done in previous works (Teufl et al., 2019b; Naeemabadi. et al., 2018).

2 MATERIALS AND METHODS

2.1 Hardware

The proposed system uses wearable IMUs that are attached to the body segments as shown in Fig. 1. The hardware consists of a set of 7 Xsens MTw Awinda units (Paulich et al., 2018), shown in Fig. 2 A. Data from the accelerometer and gyroscope is captured at a sampling frequency of 1000 Hz and low-pass filtered at a bandwidth of 184 Hz. In this application the movements are sampled at 100 Hz, with a latency of 30 ms. The weight of each sensor is 16 g.

The optical tracking was performed with 9 Optitrack Flex 13 cameras at 120 Hz, data were collected and analyzed with MotiveBody (https://optitrack.com). A set of 5 reflective marker was attached to each of the IMUs. The markers were connected with a rigid structure shown in Fig. 2 B.

The support surface movement was implemented with the 6 DOF device PS-6TM-150 from Motionsystems (www.motionsystems.eu) controlled with a custom software. The support plate is 80×80 cm and the subject is standing on its center. The 3D rendering of the platform is shown in Fig. 2 C.

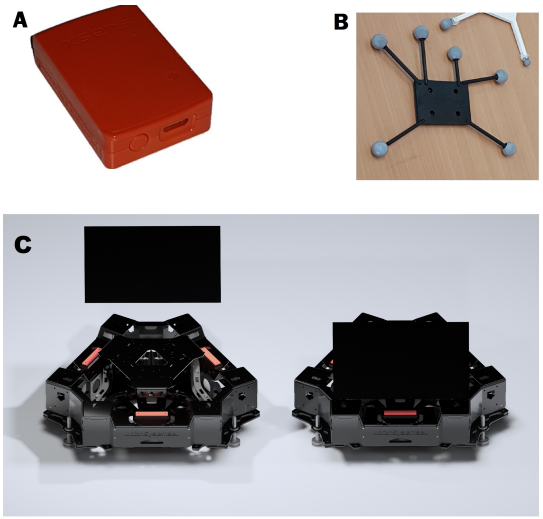

Figure 2: Overview of the hardware components.(A) The IMU. (B) The reflective markers. (C) A render of the moving support surface platform. On the left the 80×80 cm support surface has been lifted to show the structure of the moving platform.

2.2 Tracking Algorithm

The algorithm used to track the lower limbs is similar to the one presented in (Laidig et al., 2019) for the tracking of human hands. The sensors are fixed as shown in Fig 1. It is assumed that the joints are move like a hinge joint following the work presented in (Laidig et al., 2019) and (Laidig et al., 2017b). This assumption is not true for the general range of motion of human lower limbs, both because of multiple DoF joints (e.g. the hip) and because of the elastic nature of human tissues (that means that also the knee is not strictly 1 DoF). Nevertheless this assumption is reasonable in the context of the presented posture control experiment where body sway in the sagittal plane is analyzed. Consider the tracking of two rigid bodies, $\mathcal{B}_1$ and $\mathcal{B}_2$, connected by a one-dimensional hinge joint, like the thigh and the shank in the example in Fig. 1, there is an IMU fixed to each rigid body, the relative orientation of the IMUs is not known *a priori*. The orientations are represented by the quaternions ${}^{\mathcal{B}_1}_{\mathcal{E}_1}\mathbf{q}$ and ${}^{\mathcal{B}_2}_{\mathcal{E}_2}\mathbf{q}$ where the subscript denotes the frame of reference and the superscript denotes the frame of interest. Due to the nature of the sensors, i.e. 6D IMUs, the heading component of each orientation is unknown. This is modeled as if the orientations are estimated in the two reference frames $\mathcal{E}_1$ and $\mathcal{E}_2$. As only the heading is affected and the inclination can

be correctly estimated by the accelerometer and gyroscope, the difference between $\mathcal{E}_1$ and $\mathcal{E}_2$ is only the rotation ${}^{\mathcal{E}_1}_{\mathcal{E}_2}\mathbf{q}(t,\delta)$ around the global vertical axis. The angle of this rotation is called heading offset and is denoted by $\delta(t)$(Laidig et al., 2019). Knowing this angle yields the relative orientation ${}^{\mathcal{B}_1}_{\mathcal{B}_2}\mathbf{q}$ of the two bodies with

$$ {}^{\mathcal{B}_2}_{\mathcal{B}_1}\mathbf{q} = {}^{\mathcal{B}_2}_{\mathcal{E}_1}\mathbf{q}^{-1} \otimes {}^{\mathcal{E}_2}_{\mathcal{E}_1}\mathbf{q}(t,\delta) \otimes {}^{\mathcal{B}_2}_{\mathcal{E}_2}\mathbf{q} \quad (1) $$

the basic idea to estimate the value of $\delta(t)$ is that the relative orientation ${}^{\mathcal{B}_1}_{\mathcal{B}_2}\mathbf{q}$ of a one-dimensional joint is limited to rotations around one well-defined joint axis, as shown in Fig.1 for the knee joint. Following Eq. 1,the relative orientation can be formulated as a function of $\delta(t)$ with ${}^{\mathcal{B}_1}_{\mathcal{B}_2}\mathbf{q} = f(t,\delta)$. It is then possible to find an Euler angles decomposition of ${}^{\mathcal{B}_2}_{\mathcal{B}_1}\mathbf{q}(t,\delta)$such that the first angle corresponds to the joint angle (Laidig et al., 2019). The angles of the decomposition are denoted by α,β and γ. Then the following constraint holds:

$$ |\beta(t,\delta)| + |\gamma(t,\delta)| = 0 \quad (2) $$

The heading offset $\delta(t)$ is a scalar variable that can be estimated using a sliding window optimization method based on the constraint 2 with the cost function

$$ e(\delta) = \sum_{k=1}^{N} \beta(t,\delta)^2 + \gamma(t,\delta)^2 \quad (3) $$

where t_k being is sample index in a time-window with N samples. This is computed repeatedly on overlapping time windows to obtain the estimator $\hat{\delta}(t)$ for the heading offset. In the presented case the hip orientation, ${}^{\mathcal{H}}\mathbf{q}$, is taken as reference and the corrected orientations are computed applying Eq. 1 through the kinematic chains of the legs. The orientations of the right thigh, ${}^{\mathcal{RT}}\mathbf{q}$, and left thigh, ${}^{\mathcal{LT}}\mathbf{q}$, given the respective heading correction angles $\delta_{\{\mathcal{R}|\mathcal{L}\}T}$ Eq. 1 becomes

$$ {}^{\{\mathcal{R}|\mathcal{L}\}T}_{\mathcal{H}}\mathbf{q} = {}^{\mathcal{H}}_{\mathcal{E}_1}\mathbf{q}^{-1} \otimes {}^{\mathcal{E}_2}_{\mathcal{E}_1}\mathbf{q}(t,\delta_{\{\mathcal{R}|\mathcal{L}\}T}) \otimes {}^{\{\mathcal{R}|\mathcal{L}\}T}_{\mathcal{E}_2}\mathbf{q} \quad (4) $$

The calculated $\delta_{\{\mathcal{R}|\mathcal{L}\}T}$ is used to correct the thighs quaternions by rotating the reference frames of the thighs, $\mathcal{E}_2$, onto the reference frame of the hip $\mathcal{E}_1$ is

$$ {}^{\{\mathcal{R}|\mathcal{L}\}T}_{\mathcal{E}_1}\mathbf{q} = {}^{\mathcal{E}_2}_{\mathcal{E}_1}\mathbf{q}(t,\delta_{\{\mathcal{R}|\mathcal{L}\}T}) \otimes {}^{\{\mathcal{R}|\mathcal{L}\}T}_{\mathcal{E}_2}\mathbf{q} \quad (5) $$

The same procedure is applied to the shank and the foot segments.

2.3 Posture Control Analysis

The proposed tracking system aims to the development of posture control experiments that allows the comparison of human and robot responses (Torricelli et al., 2020; Mergner and Lippi, 2018; Torricelli et al., 2014). For this purpose the evaluation of the system consist of a frequency domain analysis of the body sway response induced by the external stimulus performed in typical human and humanoid posture control experiments(Peterka, 2002; Mergner et al., 2009; Mergner, 2010; Lippi and Mergner, 2017) . The support surface tilt profile is a pseudo-random ternary sequence stimulus (PRTS), introduced by (Peterka, 2002). The signal profile is shown in Fig. 3. This signal prevents humans and humanoids from using prediction, that can affect strongly posture control (Martínez et al., 2014; Lippi, 2018). The power-spectrum of the PRTS allows for the evaluation of gain, phase, and coherence of the disturbance-evoked body segments excursions (Mergner and Lippi, 2018). The FRF is evaluated for COM sway (BS) and the sway of specific body segments (LS,TS). BS is not measured directly but computed from LS and TS assuming human body mass distribution from (Winter, 2009) as

$$ BS = sin^{-1}\left(\frac{(m_T l_L + m_L h_L)sin(LS) + h_T m_T sin(TS)}{h_B m_B}\right) \quad (6) $$

where m_T is the mass of the trunk, m_L the mass of the legs and $m_B = m_T + m_L$ the mass of the body excluding the feet. the mass distribution is defined by the ratios $m_T/m_B = 0.6982$ and $m_L/m_B = 0.3018$ and by the ratio between the height of the COM of the respective segments, $h_B = 0.9684$ for the whole body, $h_L = 0.4753$ for the leg and $h_T = 0.3173$ for the trunk. The leg length from ankle to hip was $l_L = 0.8642$.

The FRFs are estimated transfer functions between the stimulus (FS) and the sway responses (LS,TS,BS). The signals are transformed through *discrete Fourier transform*, and the transfer function is computed as the ratio between the cross-power spectrum of the input X and the output y and transform of the input signal i.e.

$$ H(f) = \frac{G_{XY}(f)}{G_X(f)} \quad (7) $$

Coherence is calculated as the squared cross-power spectrum divided by the product of sway response and stimulus power spectra. it varies from 0 to 1, where 0 indicates that there is no linear correlation between the stimulus and response, and 1 represents a perfect linear correlation. Both the presence of noise and nonlinear relationships between input and output

lead to coherence smaller than 1 (Bendat and Piersol, 2011).

The data are obtained through a single trial with one subject (female, 30 years old, 176 cm tall) standing upright with eyes open on the platform. The study was in accordance with the 1964 Helsinki Declaration in its latest revision. Both the FRF (gain and phase) and the coherence are computed and plotted over a set of frequency of interest where the spectrum of PRTS function has its peaks (see Fig.4).

3 RESULTS AND DISCUSSION

A comparison in time domain between the support surface tilt and the foot orientation FS, that represent the last element in the kinematic chain is shown in Fig. 3. There are some small tracking errors on the absolute position, specifically a $RMSE = 0.0094°$. Most of the tracking error on FS is represented by high frequency disturbance and appears to be concentrated on specific samples, e.g. around 150 s. A comparison of the two signals in frequency domain is shown in Fig. 4. The comparison confirms that the most of the difference between the stimulus and the tracked FS is represented by differences at higher frequencies.

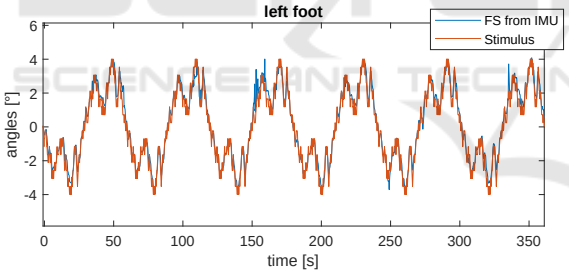

Figure 3: Support Surface tracking using the reconstruction of left foot position. The stimulus is the PRTS used as reference for the platform, the foot rotation FS has been centered around the rest value of 49° so that an angle of 0° means that the support surface is horizontal.

The frequency response functions describing the sway of body segments, leg (LS) and trunk (TS), and center of mass (BS) are shown in Fig. 5 in comparison with the same function obtained with the optical tracking in Fig. 6. In this scenario the subject was not using the knee joints and hence LS and SS are equivalent. The two measures are in agreement over the frequency of interests and exhibit some smaller differences at higher frequencies, i.e. a difference can be observed in the gain and the phase above 1 Hz. The implication of Eq. 7 is that the power-spectrum of the output at frequencies where the stimulus is zero is

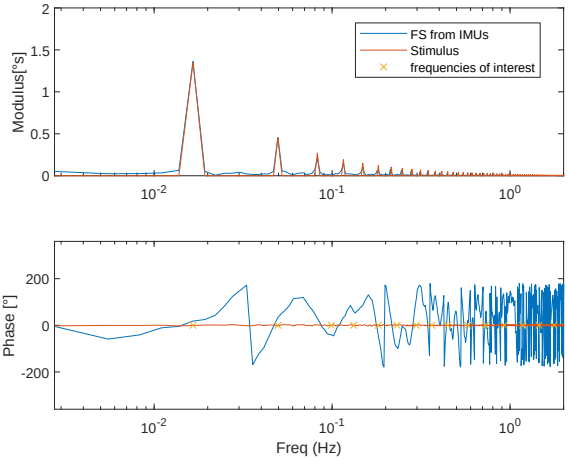

Figure 4: Representation in frequency domain of the PRTS profile (*Stimulus*, in orange) and the foot in space orientation tracked by the IMUs (*FS*, in blue). There is some tracking error, most of it not associated with the frequencies of interest where the PRTS spectrum has its peaks.

not relevant. The FRF is computed and plotted only for the frequencies where the PRTS spectrum is not zero. This means that not all the error observed in time domain, showed in Fig. 3, is reflected in the result showed in Fig. 5.

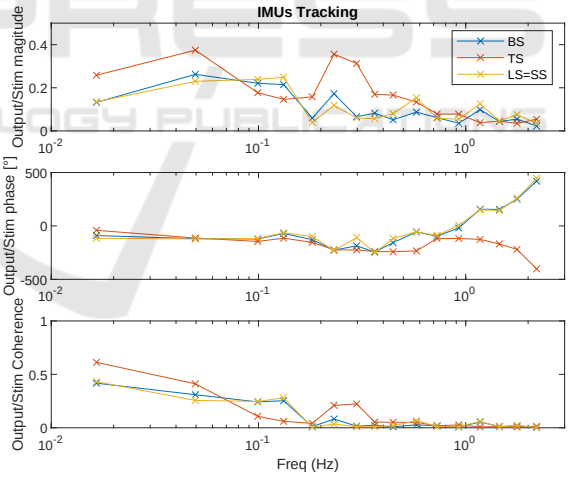

Figure 5: Frequency response functions (FRFs) body for segments and body COM sway computed using the IMUs tracking. The profile is similar to the one produced by optical tracking (compare Fig. 6). The effect of measurament noise is visible mainly at 1 Hz on LS and BS.

4 CONCLUSIONS AND FUTURE WORK

The presented magnetometer-free tracking system based on IMUs has been evaluated performing a trial

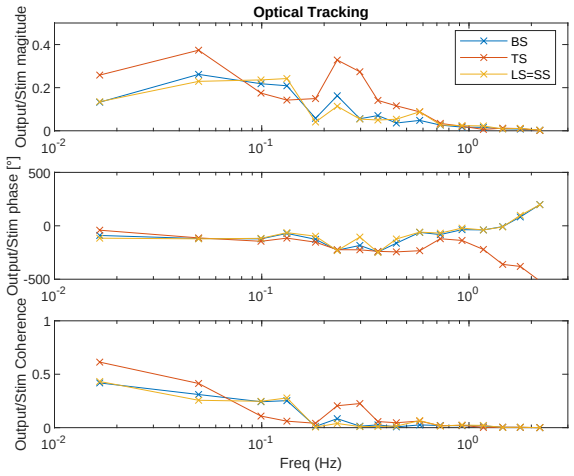

Figure 6: Frequency response functions (FRFs) body for segments and body COM sway computed using the optical tracking. Notice the absence of the small peak above 1 Hz that can be observed in Fig. 5. Also the phase presents some differences at higher frequencies.

and a typical frequency domain analysis required for human and humanoid posture control experiments. The system proved to be suitable for the analysis of posture control experiments, in the sense that the FRFs obtained for body segment sway were similar to the ones obtained using optical tracking. Future work will aim to the integration in the framework of the EUROBENCH project,in order to use it for other experiments proposed within the consortium. In particular, the presented posture control analysis is based on a reconstructed body position (TS,LS,BS). For this purpose the system should be interchangeable with other systems used within the consortium, like *wearHEALTH* (Teufl et al., 2019b; Teufl et al., 2019a), and allow for the comparison of experimental results obtained with the different tracking systems. The implementation of the system will be updated to a sample rate of 100 Hz. During the developed of the system, gait tracking was also tested. The analysis of gait will be one possible additional use of the system within the EUROBENCH consortium.

ACKNOWLEDGEMENTS

This work is supported by the project COMTEST (Lippi et al., 2019b), a subproject of EUROBENCH (European Robotic Framework for Bipedal Locomotion Benchmarking, www.eurobench2020.eu) funded by H2020 Topic ICT 27-2017 under grant agreement number 779963. Thanks to Giorgio Castellano for the 3D render of the platform.

REFERENCES

Bendat, J. S. and Piersol, A. G. (2011). *Random data: analysis and measurement procedures*, volume 729. John Wiley & Sons.

Buke, A., Gaoli, F., Yongcai, W., Lei, S., and Zhiqi, Y. (2015). Healthcare algorithms by wearable inertial sensors: a survey. *China Communications*, 12(4):1–12.

De Vries, W., Veeger, H., Baten, C., and Van Der Helm, F. (2009). Magnetic distortion in motion labs, implications for validating inertial magnetic sensors. *Gait & posture*, 29(4):535–541.

Fong, D. T.-P. and Chan, Y.-Y. (2010). The use of wearable inertial motion sensors in human lower limb biomechanics studies: a systematic review. *Sensors*, 10(12):11556–11565.

Hauser, H., Neumann, G., Ijspeert, A. J., and Maass, W. (2011). Biologically inspired kinematic synergies enable linear balance control of a humanoid robot. *Biological cybernetics*, 104(4-5):235–249.

Hettich, G., Lippi, V., and Mergner, T. (2013). Human-like sensor fusion mechanisms in a postural control robot. In Londral, A. E., Encarnacao, P., and Pons, J. L., editors, *Proceedings of the International Congress on Neurotechnology, Electronics and Informatics. Vilamoura, Portugal*, pages 152–160.

Hettich, G., Lippi, V., and Mergner, T. (2015). Human-like sensor fusion implemented in the posture control of a bipedal robot. In *Neurotechnology, Electronics, and Informatics*, pages 29–45. Springer.

Laidig, D., Lehmann, D., Bégin, M.-A., and Seel, T. (2019). Magnetometer-free realtime inertial motion tracking by exploitation of kinematic constraints in 2-dof joints. In *2019 41st Annual International Conference of the IEEE Engineering in Medicine and Biology Society (EMBC)*, pages 1233–1238. IEEE.

Laidig, D., Müller, P., and Seel, T. (2017a). Automatic anatomical calibration for imu-based elbow angle measurement in disturbed magnetic fields. *Current directions in biomedical engineering*, 3(2):167–170.

Laidig, D., Schauer, T., and Seel, T. (2017b). Exploiting kinematic constraints to compensate magnetic disturbances when calculating joint angles of approximate hinge joints from orientation estimates of inertial sensors. In *2017 International Conference on Rehabilitation Robotics (ICORR)*, pages 971–976. IEEE.

Leardini, A., Chiari, L., Croce, U. D., and Cappozzo, A. (2005). Human movement analysis using stereophotogrammetry: Part 3. soft tissue artifact assessment and compensation. *Gait & Posture*, 21(2):212 – 225.

Lippi, V. (2018). Prediction in the context of a human-inspired posture control model. *Robotics and Autonomous Systems*.

Lippi, V. and Mergner, T. (2017). Human-derived disturbance estimation and compensation (dec) method lends itself to a modular sensorimotor control in a humanoid robot. *Frontiers in neurorobotics*, 11:49.

Lippi, V., Mergner, T., Seel, T., and Maurer, C. (2019a). Benchmarking humanoid postural control–techniques

and technologies inspired by human experiments. In *IEEE Humanoids Workshop on: performance indicators and benchmarking facilities for bipedal locomotion, IEEE-RAS 19th International Conference on Humanoid Robots (Humanoids)*.

Lippi, V., Mergner, T., Seel, T., and Maurer, C. (2019b). COMTEST project: A complete modular test stand for human and humanoid posture control and balance. In *2019 IEEE-RAS 19th International Conference on Humanoid Robots (Humanoids) Toronto, Canada. October 15-17*.

Martínez, S., Esteban, D., Jardón, A., and Balaguer, C. (2014). Anticipative humanoid postural control system for locomotive tasks. In *2014 IEEE-RAS International Conference on Humanoid Robots*, pages 146–151.

Mergner, T. (2010). A neurological view on reactive human stance control. *Annual Reviews in Control*, 34(2):77–198.

Mergner, T. and Lippi, V. (2018). Posture control human-inspired approaches for humanoid robot benchmarking: Conceptualizing tests, protocols and analyses. *Frontiers in Neurorobotics*, 12:21.

Mergner, T., Schweigart, G., and Fennell, L. (2009). Vestibular humanoid postural control. *Journal of Physiology - Paris*, 103:178–194.

Miller, N., Jenkins, O. C., Kallmann, M., and Mataric, M. J. (2004). Motion capture from inertial sensing for untethered humanoid teleoperation. In *4th IEEE/RAS International Conference on Humanoid Robots, 2004.*, volume 2, pages 547–565. IEEE.

Müller, P., Bégin, M.-A., Schauer, T., and Seel, T. (2016). Alignment-free, self-calibrating elbow angles measurement using inertial sensors. *IEEE journal of biomedical and health informatics*, 21(2):312–319.

Naeemabadi., M., Dinesen., B., Andersen., O. K., Najafi., S., and Hansen., J. (2018). Evaluating accuracy and usability of microsoft kinect sensors and wearable sensor for tele knee rehabilitation after knee operation. In *Proceedings of the 11th International Joint Conference on Biomedical Engineering Systems and Technologies - Volume 1 BIODEVICES: BIODEVICES,*, pages 128–135. INSTICC, SciTePress.

Ott, C., Henze, B., Hettich, G., Seyde, T. N., Roa, M. A., Lippi, V., and Mergner, T. (2016). Good posture, good balance: Comparison of bioinspired and model-based approaches for posture control of humanoid robotsg. *IEEE Robotics & Automation Magazine*, 23(1):22–33.

Paulich, M., Schepers, M., Rudigkeit, N., and Bellusci, G. (2018). Xsens mtw awinda: Miniature wireless inertial-magnetic motion tracker for highly accurate 3d kinematic applications. *Xsens: Enschede, The Netherlands*.

Peterka, R. (2002). Sensorimotor integration in human postural control. *Journal of neurophysiology*, 88(3):1097–1118.

Salehi., S. and Stricker., D. (2020). Validation of a low-cost inertial exercise tracker. In *Proceedings of the 9th International Conference on Sensor Networks - Volume 1: SENSORNETS,*, pages 97–104. INSTICC, SciTePress.

Seel, T., Raisch, J., and Schauer, T. (2014). Imu-based joint angle measurement for gait analysis. *Sensors*, 14(4):6891–6909.

Seel, T. and Ruppin, S. (2017). Eliminating the effect of magnetic disturbances on the inclination estimates of inertial sensors. *IFAC-PapersOnLine*, 50(1):8798–8803.

Teufl, W., Lorenz, M., Miezal, M., Taetz, B., Fröhlich, M., and Bleser, G. (2019a). Towards inertial sensor based mobile gait analysis: Event-detection and spatio-temporal parameters. *Sensors*, 19(1):38.

Teufl, W., Miezal, M., Taetz, B., Fröhlich, M., and Bleser, G. (2019b). Validity of inertial sensor based 3d joint kinematics of static and dynamic sport and physiotherapy specific movements. *PloS one*, 14(2).

Torricelli, D., Mizanoor, R. S., Gonzalez, J., Lippi, V., Hettich, G., Asslaender, L., Weckx, M., Vanderborght, B., Dosen, S., Sartori, M., et al. (2014). Benchmarking human-like posture and locomotion of humanoid robots: A preliminary scheme. In *Conference on Biomimetic and Biohybrid Systems*, pages 320–331. Springer.

Torricelli, D., Mizanoor, R. S., Lippi, V., Weckx, M., Mathijssen, G., Vanderborght, B., Mergner, T., Lefeber, D., and Pons, J. L. (2020). Benchmarking human likeness of bipedal robot locomotion: State of the art and future trends. In *Metrics of Sensory Motor Coordination and Integration in Robots and Animals*, pages 147–166. Springer.

Winter, D. A. (2009). *Biomechanics and motor control of human movement*. John Wiley & Sons.

Wong, C., Zhang, Z.-Q., Lo, B., and Yang, G.-Z. (2015). Wearable sensing for solid biomechanics: A review. *IEEE Sensors Journal*, 15(5):2747–2760.

Zebenay, M., Lippi, V., and Mergener, T. (2015). Human-like humanoid robot posture control. In *2015 12th International Conference on Informatics in Control, Automation and Robotics (ICINCO)*, volume 2, pages 304–309. INSTICC, SciTePress.